Open Archive Toulouse Archive Ouverte (OATAO)

OATAO is an open access repository that collects the work of some Toulouse researchers and makes it freely available over the web where possible.

This is an author's version published in: https://oatao.univ-toulouse.fr/28371

Official URL: https://doi.org/10.2514/6.2021-0388

To cite this version :

Awes Cheynis, Amaury and Daon, Renaud and Dufour, Guillaume and Carbonneau, Xavier and Marty, Julien and Barrier, Raphael Unsteady Body Force Methodology for Fan Operability Assessment under Clean and Distorted Inflow Conditions. (2021) In: AIAA SciTech Forum, 11 January 2021 - 15 January 2021 (Virtual Event).

Any correspondence concerning this service should be sent to the repository administrator: tech-oatao@listes-diff.inp-toulouse.fr

AIAA SciTech Forum
11–15 & 19–21 January 2021, VIRTUAL EVENT
AIAA Scitech 2021 Forum
10.2514/6.2021-0388

Unsteady Body Force Methodology for Fan Operability Assessment under Clean and Distorted Inflow Conditions

Amaury Awes* and Renaud Daon*
Safran Aircraft Engines, Moissy-Cramayel, France

Guillaume Dufour† and Xavier Carbonneau†
ISAE-SUPAERO, Université de Toulouse, France

Julien Marty‡ and Raphaël Barrier‡
ONERA - The French Aerospace Lab, Meudon, France

With more complex aircraft architectures, fast and cost-effective design iterations are key to improve overall fuel efficiency. This paper proposes to revisit a low-order unsteady modeling approach to replace costly full annulus URANS simulation. Unsteady Body Force Methods (UBFM) could allow a significant cost reduction for fan distortion ingestion and operability assessment. In this approach, the bladed area in the computational domain is replaced by source terms in the Navier–Stokes equations, and the cost of the simulation is reduced by a factor of 26. The operability of the fan is evaluated with and without distortion in order to assess the accuracy of the model. Previously published results of URANS simulations performed on the same fan subject to an unsteady vortex ingestion are used as reference.[1] The results show that our UBFM is able to predict rotating stall cells, with patterns and rotating speed similar to the URANS data.

Nomenclature

b	Blockage factor [-]
BL(I)	Boundary Layer (Ingestion)
BPR	ByPass Ratio
CFD	Computational Fluid Dynamics
δ	Local flow deviation angle [°]
δ_0	Reference deviation angle at maximum efficiency [°]
FFT	Fast Fourier Transform
f_n	Body-force component normal to the relative flow [N/kg]
f_p	Body-force component parallel to the relative flow [N/kg]
h	Effective blade to blade staggered spacing [m]
h/H	Relative spanwise position [-]
K_{p0}	Friction drag coefficient at maximum efficiency [-]
λ	Throttle law coefficient [Pa]
$\dot{m}$	Massflow [kg/s]
M_{rel}	Relative Mach number [-]
Nn	Nominal rotational speed [-]
N_{qo}	Timestep refinement factor [-]
OGV	Outlet Guide Vane

*Department of Engineering Research & Technology, Safran Aircraft Engines
†Université de Toulouse, ISAE-SUPAERO
‡Applied Aerodynamics Department, ONERA

π	Total pressure ratio [-]
Re_x	Local chordwise Reynolds number
TM	Throttle Margin [%]
θ	Angular position $[rad]$
(U)RANS	(Unsteady)Reynolds-Averaged Navier–Stokes
$V_{t/m/x}$	Tangential/Meridional/Axial velocity $[m/s]$
w	Relative flow velocity [m/s]

I. Introduction

With the global trend to reduce the environmental impact of aviation, new aircraft designs, and propulsion architectures are being investigated. The necessity to perform fast and efficient numerical simulations is paramount and given the complexity of some integrations, existing approaches may be challenged. Indeed, some concepts such as Boundary Layer Ingesting fans (BLI)[2,3,4,5] are purposely introducing distortion to the fan, resulting in an increase of the overall aircraft fuel efficiency. Simulating such cases requires full annulus URANS computations to deal with the non-axisymmetric inflow. Some additional unsteady effects are a byproduct of the current trend of increasing the bypass ratio of turbofans, which results in engines having lower ground clearances, possibly leading to a stronger ground vortex.[6] Finally, another consequence of higher BPRs is the fact that due to weight concerns, inlet cowls are being shortened and therefore are less efficient in shielding the fan from crosswind distortions.[7,8] For all these examples, full annulus URANS computations are not suited for fast design iterations. An alternative is the use of low-order modeling to effectively evaluate a design, preferably with minimal calibration data. A possible suitable candidate is the use of the Body Force Method, in which the bladed engine sections are modeled by source terms to the Navier–Stokes equations, instead of explicitly meshing the blades.

Multiple formulations for the source terms have been proposed in the literature. All formulations are based on Marble's decomposition of the flow,[9] where normal and parallel forces are applied to the flow. The philosophy of this approach is that the body forces locally react to perturbations in the flow field. Gong first formulated a BFM modeling in his PhD.[10] This model requires numerous reference CFD computations for calibration. A second approach was proposed by Thollet, with an analogy with a lift and drag formulation.[11] The calibration process is much improved compared to Gong's formulation, which was found to be not as robust. Moreover, the Lift/Drag model requires reference data only for a single operating point, whereas multiple points are required for the first model. This second model has two main limitations, a manual calibration coefficient is still mandatory for capturing the choke massflow, and the model lacks physics-based modeling in the parallel force, which biases the spanwise distribution of the flow. Another approach is the Hall–Thollet model,[12,11] which only requires the blade geometry and can be self-calibrated with the a priori knowledge of a best-efficiency point.

Regarding the characterization of the stability of a compressor, Day and Camp[13,14] showed two types of rotating stall development, modal and spike stall. Modal stall is characterized by a long length scale disturbance in the flow-field occurring at the peak of the total-to-static pressure ratio. The second type of stall inception is the spike stall. Vo et al.[15,16] have shown that the origin of a spike involves the leading-edge flow spillage that sheds into a vortex that spills onto the next blade. This then triggers the next blade vortex shedding due to the local increase in incidence and causes a rapid propagation leading to a generalized stall within a few rotations. A second well-established criterion is the trailing-edge flow impingement. Part of the tip-clearance flows impinges into the adjacent blade passage at the trailing edge on the pressure surface of the blade, leading to rotating stall. Recently, Perovic et al.[17] have discussed a criterion for operability under BLI distortion, where a spike disturbance seen in one channel must be dissipated before the next encounter of the affected sector. Failure to do so amplifies the spike and therefore leads to stall. This criterion was found to be also valid in a vortex distortion.[1] Despite the latter, no criteria is universally accepted for defining the operability limit, neither under steady nor unsteady distortions.

Regarding the application range of the body force method, all the models mentioned above have been successfully applied in the past few years for various purposes related to fan integration, such as fan–intake interactions for short inlet or BLI fan performance effects, using a steady approach. In contrast, the use of unsteady body force modeling for rotating stall predictions has received considerably less attention: only Gong's approach was used, in the case of single [18] or multi-stage compressors .[19] It should be emphasized

here that the version of Gong's model used in those studies (i) is a low-speed approach, not suited for flows with compressibility effects, (ii) relies on non-local formulation that requires a dedicated solver and (iii) was not applied to fans.

In this context, the first goal of the paper is to revisit the use of unsteady body force modeling, using recent BF models, for the simulation of rotating stall inception. A second goal is to specifically focus on the assessment of the prediction of the operability of the fan stage of a modern turbofan. Finally, the impact of inflow distortions, such as a steady or a fluctuating vortex, will be examined.

II. Test Case

II.A. MASCOT2

The MASCOT2 test-case, shown in Figure 1, is an 18 fan blade Safran Aircraft Engines – General Electric full-scale turbofan demonstrator. It has undergone a complete test campaign including performance, acoustic, operability and cross-wind tests. It provides a valuable database to validate numerical results.

Figure 1: MASCOT2 fan

II.B. Reference Data

The reference data used in this paper to assess the UBFM results is a previous study using full annulus URANS simulations.[1] This analysis characterized the operability of MASCOT2 under clean inflow and vortex ingestion. The limit was defined using the first signs of rotating stall inception. The vortex was representative of a ground vortex. The unsteadiness of the vortex was also introduced and the impact was characterized.

III. Model Presentation

The BFM used in this paper is the Hall–Tholet model.[20,12,11] The blade effects are introduced into the flow with source terms computed using the blade geometry data and the local flow information. Two forces are introduced, one normal and the other parallel to the relative flow vector w. The normal force f_n reflects the blade deviation and loading. The parallel force f_p is proportional to the entropy gradient which is associated with the losses.

$$f_n = \frac{1}{2}w^2 2\pi\frac{\delta}{hb} \Rightarrow \begin{cases} \frac{1}{2}w^2 2\pi\frac{\delta}{hb}\frac{1}{\sqrt{1-{M_{rel}}^2}} & \text{if } M_{rel} < 1 \\ \frac{1}{2}w^2 2\pi\frac{\delta}{hb}\frac{1}{2\pi\sqrt{{M_{rel}}^2-1}} & \text{if } M_{rel} > 1 \end{cases} \tag{1}$$

Equation 1 expresses the normal force applied in the domain. Where h is the effective blade-to-blade staggered spacing, b is the blockage factor, and M_{rel} is the relative Mach number. This formulation was modified by Thollet to incorporate a correction for the metal blockage, as well as compressibility effects using the Prandtl-Glauert (subsonic) and Ackeret (supersonic) corrections.

$$f_p = \frac{w^2}{2hb}[K_{p0} \times Re_x^{0.2} + 2\pi(\delta - \delta_0)^2] \tag{2}$$

Equation 2 expresses the parallel force applied in the domain. δ is the local flow deviation angle, and δ_0 is the reference deviation angle at maximum efficiency. K_{p0} is a calibration coefficient representing friction coefficient, and Re_x is the local chordwise Reynolds number.

The CFD simulations are performed using the ONERA elsA CFD software.[21] Spatial discretization is performed with a second-order Roe scheme, and the k–l Smith turbulence model is used. The steady BFM computations are done on a single sector with an implicit pseudo-time marching approach.

The UBFM computations are performed on a whole-annulus domain and integrated in time with the 2nd order Gear scheme with Newton sub-iterations. The mesh topology is shown in Figure 2. The mesh is entirely in the fixed (non-rotating) domain. The body forces are applied in two 360-degree mesh blocks representing the fan and OGV regions. A Body Force relaxation factor is also introduced.

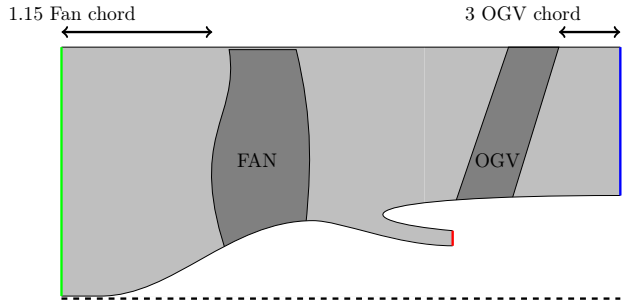

Figure 2: Schematic of the block structure of the MASCOT2 mesh (not to scale)

For all the computations, a subsonic injection is used at the inlet, and a parabolic throttle law with radial equilibrium for the outflow condition. This throttle law uses a pivot pressure defined in Equation 3 where λ is the throttle law coefficient, p_{ref} is the zero massflow pressure and $\dot{m}_{ref}$ is the nominal massflow. This λ throttle coefficient is used to virtually change the nozzle geometry without actual mesh modifications and allows a full compressor map exploration.

$$p_{pivot} = p_{ref} + \lambda \times \left(\frac{\dot{m}}{\dot{m}_{ref}}\right)^2 \tag{3}$$

IV. Preliminary Analysis

IV.A. Mesh Convergence

Mesh comparisons are done on a 36 degree sector for the steady BFM computations at 85Nn. This was the minimum sector in order to have a whole number of cells for all three meshes. The grids are generated using the Cassiopée software.[22] Three meshes are generated and labeled as "Coarse", "Medium" and "Fine" as defined in Table 1. A full performance map was performed with all 3 meshes and is shown in Figure 3.

Table 1: Summary of all the meshes tested (85Nn)

Value	Coarse	Medium	Fine
36 deg sector	1.0×10^6	2.1×10^6	2.5×10^6
360 deg domain size	10.9×10^6	22.7×10^6	25.4×10^6

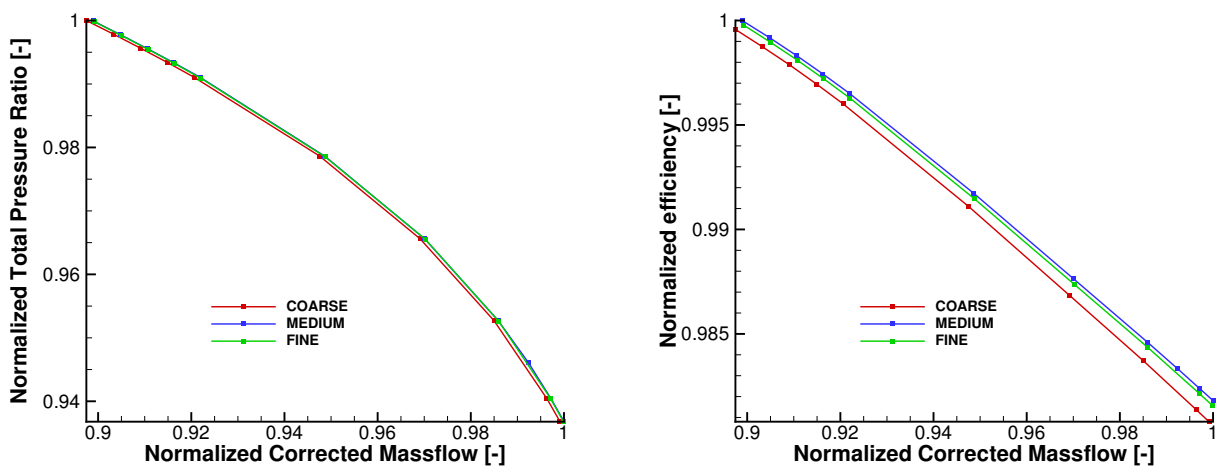

(a) Total pressure ratio comparison

(b) Efficiency comparison

Figure 3: Fan performance map comparison

These simulations did not use any calibration as the objective was to study mesh independence. All meshes showed similar results, indeed Figure 3a shows that the "Medium" and "Fine" results are superimposed and the "Coarse" is also in good agreement. Figure 3b also concurs with the "Medium" and "Fine" being converged and the "Coarse" is within less than 0.1%.

With this result, the "Medium" mesh was retained even though the "Coarse" mesh could still yield satisfactory results, particularly regarding nominal performance analysis. This decision was motivated by the requirement of this study to properly capture and discretize the ingested vortex as well as the stall inception mechanisms.

IV.B. Calibration

The accuracy of the BFM results can be improved by resorting to calibration. This calibration process involves two levers. The first is the losses in the boundary layers, which are controlled by the K_{p0} coefficient. This directly affects the maximum efficiency value and must be in agreement with the calibration data. The second is the losses due to the flow deviation, which are controlled by the δ_0 parameter. The assumption is that, at maximum efficiency, the flow deviation in regards to the blade camber line is minimal, and therefore a corrective off design term is added. The standard approach is to calibrate the boundary layer coefficient to obtain the correct maximum efficiency. The next step is to extract the flow deviation angle distribution at the maximum efficiency point and reintroduce it in the off-design term.

A novel approach proposed in this present contribution was to introduce a quadratic correction coefficient on the off-design term. This correction was chosen according to a study of the resulting error between a constant value coefficient and the URANS database. As can be observed in Figure 4 a quadratic fitting in relation to the λ coefficient can be performed. The second-order polynomial fitting ensures an excellent agreement in the region of interest, with the notable exception of the very near limit of operability, which can be attributed to the fan being near the limit of operability and therefore exhibits effects not properly captured by a 5 deg sector steady computation. This translates into a new formulation of the parallel force expressed in Equation 4. The two additional calibration coefficients are therefore a and b.

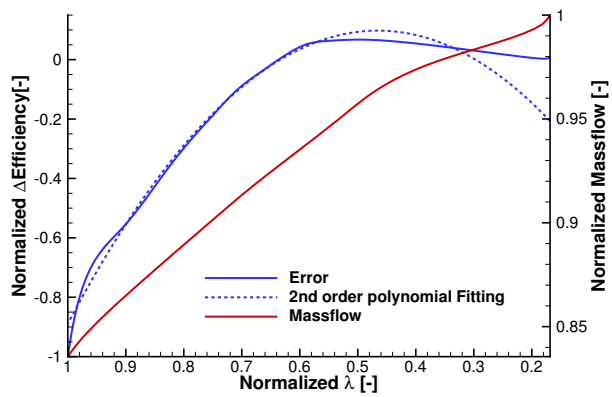

Figure 4: Error in the efficiency calculation of the BFM compared to the URANS data

$$f_p = \frac{w^2}{2hb}[K_{p0} \times Re_x^{0.2} + (a\lambda^2 + b) \times 2\pi(\delta - \delta_0)^2] \tag{4}$$

The results of this new calibration method can be observed in Figure 5. The efficiency of the fan is better predicted by the quadratic calibration and is in good agreement with the URANS data. The calibrated model shows very good agreement with the URANS data as can be observed in Figure 6. This comparison is done between the ground operating line (Normalized massflow$\approx$ 0.9) and the limit of operability, in the negative gradient region of the performance map. The axial and tangential velocity, as well as density distribution, are sub 5% for most of the span. Noticeable differences are starting at 80% span and can be attributed to the inability of the BFM model to capture shock-related effects and tip-gap flows. Finally, the most significant error can be observed in the radial velocity distribution. For both the BFM and the URANS results, the radial velocity component is negligible, and therefore minor difference equates to large relative errors.

IV.C. Time-step Convergence

In order to properly compare the UBFM results to the URANS computations, the time-step must be a multiple of 99 as it was the sampling rate used for the reference. The flow physics sought after in these computations is of low frequency. Indeed the highest frequency of the vortex is 30 Hz which is around half the fan rotational frequency. The largest time-step is therefore chosen to be 99 iterations per rotations and is

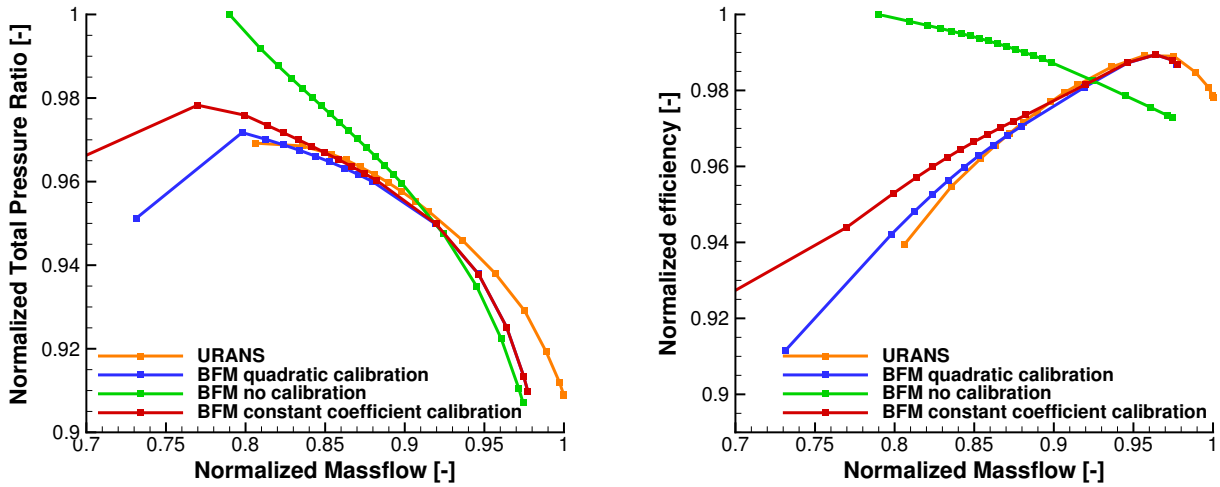

(a) Total pressure ratio comparison

(b) Efficiency comparison

Figure 5: Fan performance map comparison

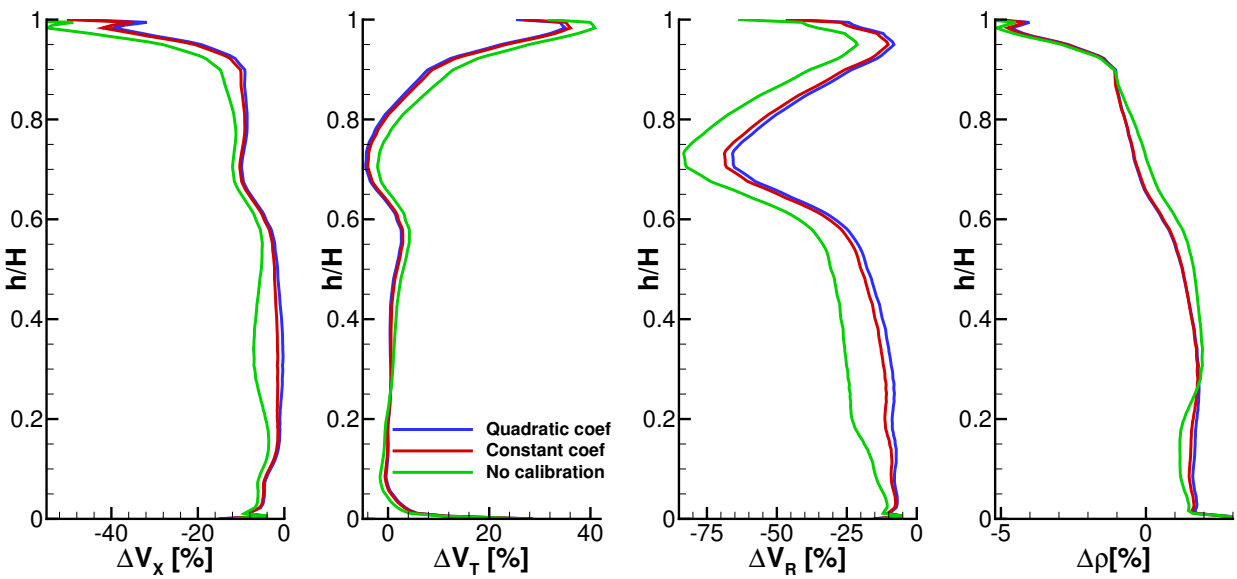

(a) Axial velocity

(b) Tangential velocity

(c) Radial velocity

(d) Density

Figure 6: Spanwise error distribution of the calibrated BFM in regards to the URANS data (Normalized massflow≈ 0.88)

referred to as $N_{qo}1$, with the medium time at 198 time-step per rotation ($N_{qo}2$) and finally, $N_{qo}3$ at 297 time-step per rotation. Three compressor maps were computed with all the time-steps. Both the $N_{qo}2$ and $N_{qo}3$ are nearly superimposed indicating convergence. The $N_{qo}1$ showed significant oscillation in the massflow. These oscillations are not damped and therefore, the $N_{qo}1$ time-step is unsuitable for the rest of this study. For the convergence analysis between the $N_{qo}2$ and $N_{qo}3$ time-steps, the firsts signs of rotating stall appeared at the same λ value and with similar massflow and total pressure values. Figures 7 and 8 show the stall analysis data with both the static pressure signals and a spatial Fast Fourier Transform to compare the harmonic content.

Figures 7a and 8a show very similar results with a stall cell rotating speed of 58% of the fan rotational speed for both the $N_{qo}2$ and $N_{qo}3$ cases. This is in good agreement with the value of 57% obtained in

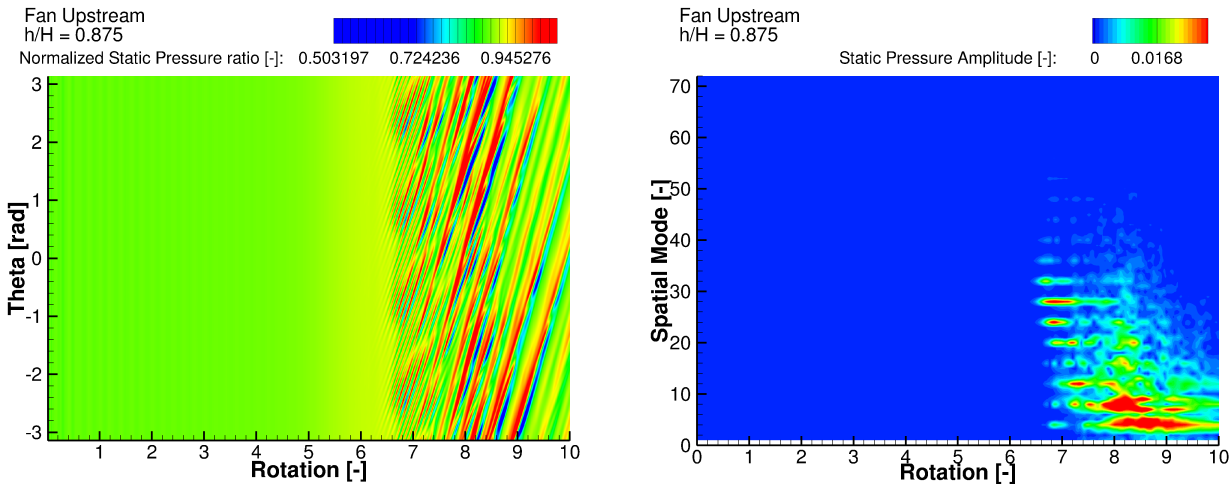

(a) Static pressure signal

(b) Spatial FFT of the signal

Figure 7: Rotating stall analysis for the $N_{qo}2$ at the $h/H = 0.875$ crown

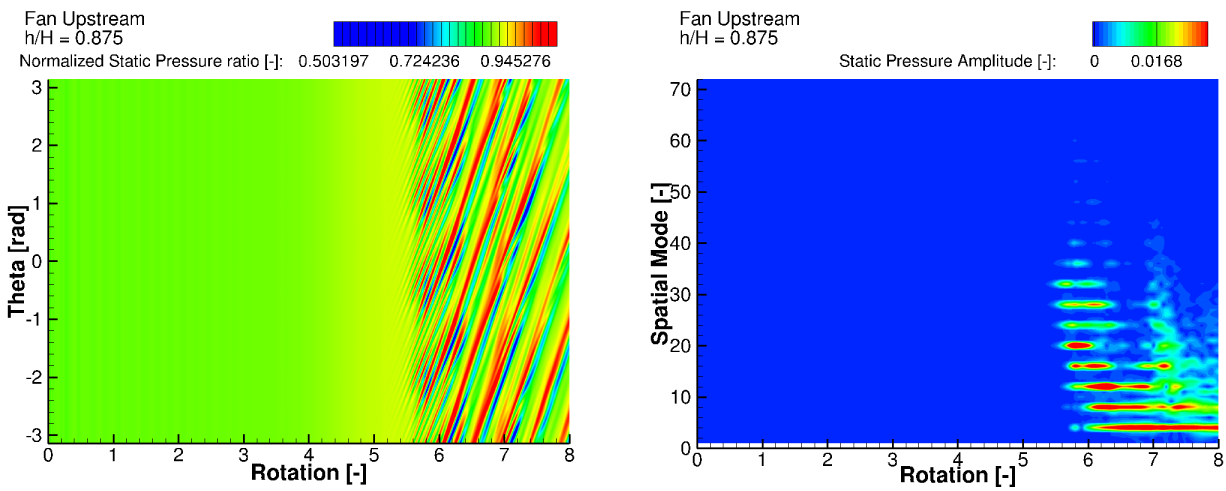

(a) Static pressure signal

(b) Spatial FFT of the signal

Figure 8: Rotating stall analysis for the $N_{qo}3$ at the $h/H = 0.875$ crown

the URANS simulations.[1] Figures 7b and 8b have the same behavior with an initial break of symmetry with a 32-lobe disturbance. The higher modes fade away into a stable 4-lobe disturbance in both cases. The two cases also share a similar characteristic with only modes multiple of 4 appearing in the rotating stall inception. This is attributed to a 4 lobe rotating stall phenomenon starting from a flow separation at the hub in the OGV row breaking axisymmetry, at 3.3 rotation as can be seen in Figure 9. The 4 lobe phenomena grows in amplitude until the effect of the fan rotating stall can be observed at 7 rotations. With the nearly superimposed performance maps from the $N_{qo}2$ and $N_{qo}3$ time-steps, as well as the very similar entry in rotating stall characteristics, the $N_{qo}2$ was chosen for the rest of this study.

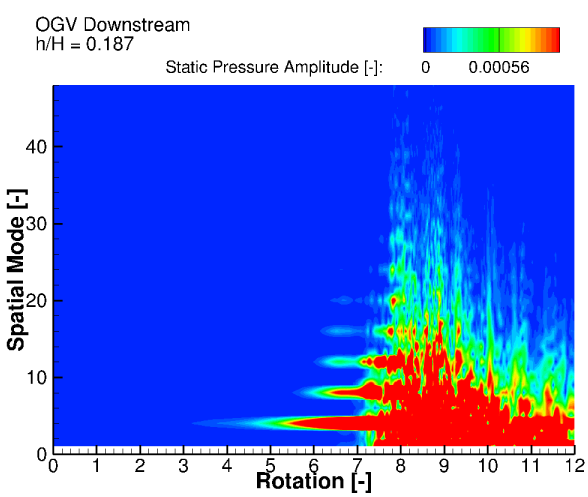

Figure 9: Spatial FFT of the signal for the $N_{qo}2$ case downstream of the OGV row

V. Clean Inflow Operability

A compressor map was computed with the UBFM approach and compared to the URANS data, as shown in Figure 10. Two limits can be defined and compared between the UBFM and the URANS. The first is the maximum total pressure ratio which is also the last point with stable massflow (in the green circles). The second point used is a one-rotation average of the massflow and total pressure ratio prior to the first signs of stall inception (in the orange circles). To quantify the loss of operability, the throttle margin (TM) defined in Equation 5 is used:

$$TM = \frac{\left(\frac{\pi}{\dot{m}}\right) - \left(\frac{\pi}{\dot{m}}\right)_{Ground\ Operating\ Line}}{\left(\frac{\pi}{\dot{m}}\right)_{Ground\ Operating\ Line}} \tag{5}$$

The throttle margin quantifies the distance between a given operating point and the reference point defined as the intersection between the engine operating line and the fan isospeed line considered.

For the maximum total pressure ratio operating point, the UBFM underpredicts the TM by 2.04%. For the stall inception point, an underprediction of 0.59% of TM can be observed, which can be considered in excellent agreement. Figure 7 shows a stall pattern rotating at 58% of the fan speed with 8 and 4 lobes, which is consistent with the URANS data as it showed an 8-10 lobe disturbance rotating at 57% of the fan speed.[1]

To conclude on the predictability of the UBFM for operability assessment, the results are highly encouraging. Indeed, the performance map is well predicted and is capable of identifying the operability limits with only 2.04% error and remains conservative. Furthermore, the entry in rotating stall remains accurate especially in terms of rotating speeds.

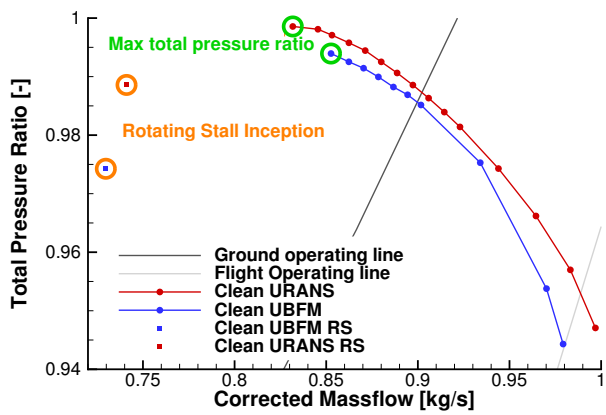

Figure 10: Total pressure ratio comparison

VI. Distortion Ingestion

VI.A. Non Fluctuating Vortex

The comparison between the URANS references and the UBFM simulations is presented in Figure 11. The throttle margin abatement due to distortion ingestion at max total pressure ratio (in green) is -3.55% between the clean and vortex for the URANS cases and -3.97% between the clean and vortex cases with the UBFM computations. This is a very promising result showing that the UBFM is capable of capturing the variation in throttle margin accurately. For the stall inception point, an excellent agreement can be observed where the throttle margin abatement is -2.13% for the URANS cases and -2.87% for the UBFM cases. Although the first signs of instability can be observed at 7.5 rotation, the rotating stall is visible starting at 8.2 rotations. Regarding the predicted rotating stall characteristics, the rotational speed is 50% of the fan speed with an initial 30-lobe motif merging into a lower 1, 2, and 8-lobe disturbance. This is in good agreement with the URANS reference,[1] which was 55% of the fan speed.

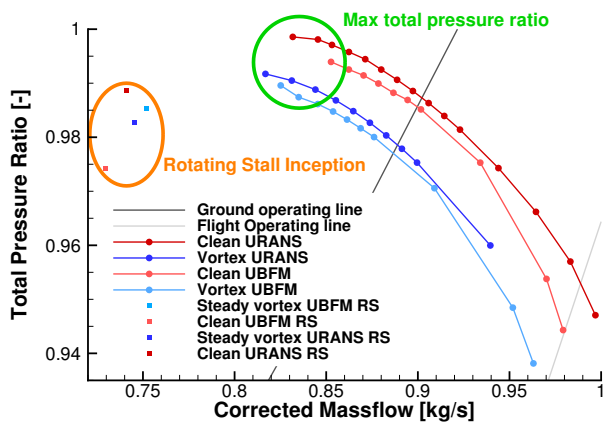

Figure 11: Total pressure ratio comparison

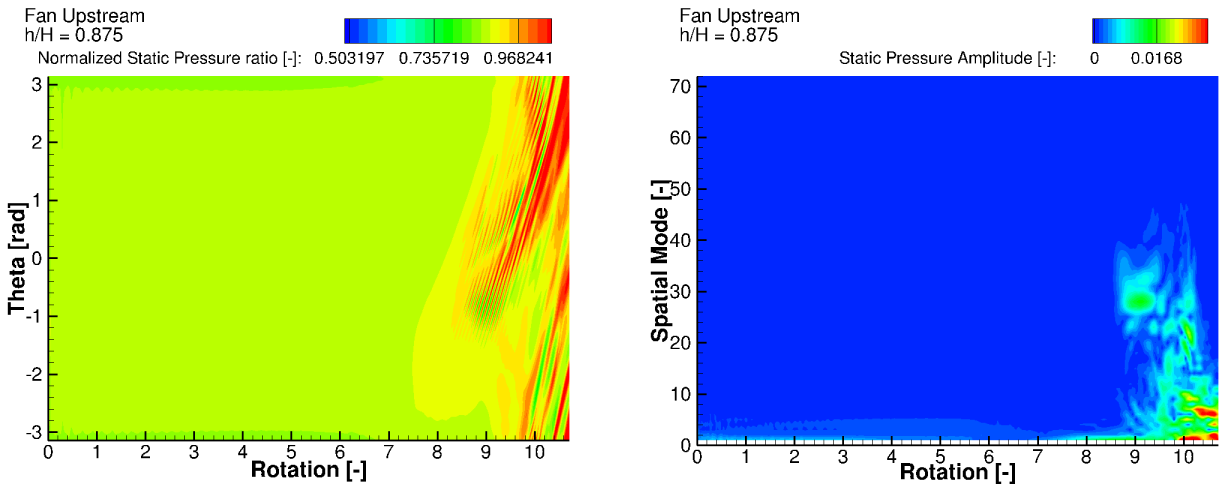

(a) Static pressure signal

(b) Spatial FFT of the signal

Figure 12: Rotating stall analysis for the steady vortex at the $h/H = 0.875$ crown

VI.B. Fluctuating Vortex

In order to assess the UBFM methodology with an unsteady distortion, a fluctuating vortex is then added. The same frequencies are used from the URANS reference cases[1] and are shown in Table 2. These are applied as a pure sinusoidal fluctuation. Moreover, a "total signal" based on a sum of all 8 frequencies mimicking the original data is tested.

Table 2: Simulated vortex frequencies

	1st Freq	**2nd Freq**	**% of variation**
Radial position	8 Hz	28 Hz	+/- 5%
Tangential position	12 Hz	28 Hz	+/- 15%
Vortex Core radius	15 Hz	36 Hz	+/- 50%
Circulation	3 Hz	30 Hz	+/- 25%

Regarding the operability of the fan under distortion, the expected response according to the URANS results[1] is no impact of the position fluctuations, but a significant impact of the circulation and vortex core radius fluctuations as they have an influence on the pressure gradients. It was also shown that the lower frequencies have a greater impact on the throttle margin than the higher frequencies. Both of these conclusions can be observed in Table 3. The impact on the λ outflow coefficient is an interesting metric as it equates to a fixed nozzle geometry and external conditions. An occurrence of stall at a reduced λ involves an earlier stall with a given geometry independently from the impact on the performance of the fan. The same conclusions cannot be obtained for the UBFM cases. Indeed, nearly all cases enter a rotating stall at the same λ value. However, the throttle margin abatement is very well predicted in every case, with a sub 1% prediction with the exception of the total signal at 1.19%. Similarly to the URANS cases, in the 3Hz circulation fluctuation, the fan enters rotating stall before the maximum value is achieved (as can be seen in Figure 15a), resulting in a possibly lower effect on the throttle margin.

Table 3: Impact of the Distortion on the Throttle Margin of the Stall Inception Operability Limit

		URANS		UBFM	
		ΔTM	λ	ΔTM	λ
Clean Inflow		0.00%	0%	-0.59%	0%
Steady Vortex		-2.13%	-4%	-2.87%	-7%
Circulation	3 Hz	-4.17%	-6%	-3.99%	-7%
	30 Hz	-4.96%	-6%	-4.00%	-7%
Vortex Core Radius	15 Hz	-8.20%	-6%	-8.50%	-7%
	36 Hz	-5.40%	-6%	-5.65%	-7%
Radial Position	8 Hz	-3.72%	-4%	-3.93%	-7%
	28 Hz	-4.29%	-4%	-4.18%	-7%
Tangential Position	12 Hz	-4.12%	-4%	-4.00%	-7%
	28 Hz	-4.26%	-4%	-4.60%	-7%
Total Signal		-3.78%	-6%	-4.97%	-7%

VII. Variation of Incidence Criterion

In the analysis of the URANS results, a criterion based on the variation of incidence was presented and showed a promising ability to predict stall inception in both clean and distorted conditions.[1] This is based on a critical swirl observed in the clean inflow case, where the incidence prior to the first signs of rotating stall is extracted over a circumferential crown and averaged. An incidence variation can then be defined with respect to the critical swirl in the clean inflow case as a difference of swirl or incidence is identical. The incidence of the distorted case is then extracted on the same crown over time. The difference between this incidence extraction and the critical value of the clean inflow case can be computed. For each timestep, the max value is extracted and the mean incidence is computed. The relative azimuthal length of the crown with supercritical incidence is also extracted at each timestep. The maximum equates to the effect of the vortex in the most affected region closest to the core. The azimuthal incidence average uses a simple arithmetic average, which reflects the overall impact on the fan. The number of azimuthal points over the critical value can be used to measure the extent of the crown beyond criticality.

Figure 13 shows the clean inflow variation of incidence at stall inception using UBFM. The affected area jumps from 0 to 100% instantly at 5.7 rotations due to the near axisymmetrical nature of the flow. 0.7 rotation after, the average and maximum value differ indicating stall inception. The critical angle used is the URANS clean inflow angle. This, therefore, shows that the UBFM can predict correctly the critical angle and therefore could be used to replace URANS simulation in order to compute the variation of incidence criterion with UBFM cases only.

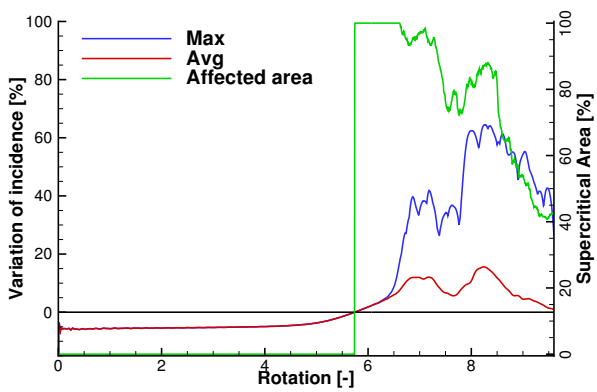

Figure 13: Variation of Incidence in a Clean Inflow Condition at Stall Inception with UBFM

With the addition of a non-fluctuating vortex, shown in Figure 14, a new phenomenon can be noted. The average is significantly lower than the maximum value (Figure 14). This is due to the averaging, which takes into account the relatively impulsionnal nature of the distortion. In this case, the affected area violently increases at 7.7 rotation and the rotating stall can be observed one rotation after. At 8.2 rotations, the average becomes positive indicating that the fan is generally operating beyond the critical incidence value.

Given the initial conclusions on the URANS and UBFM data, only the vortex circulation and core radius incidence variation are shown in Figure 15. In all the Figures but Figure 15a, the effect of the sinusoidal fluctuation can be seen on the maximum signal.

As for the URANS reference, the low-frequency circulation fluctuation incidence variation (shown in Figure 15a) shows the same behavior as the non-fluctuating vortex, suggesting that this distortion can be considered quasi-steady as the frequency is an order of magnitude lower than the fan rotation frequency. For the other cases, two trends can be observed. The first is that if the increase in the affected area happens at the peak of the fluctuation, the rotating stall can appear earlier than one rotation after. This is the case in Figures 15a,15b and 15c. The second trend is the opposite effect where the increase of the affected area happens when the distortion magnitude is reducing as in Figure 15d. In this case, the rotating stall happens 1.5 rotations after the increase in the affected area.

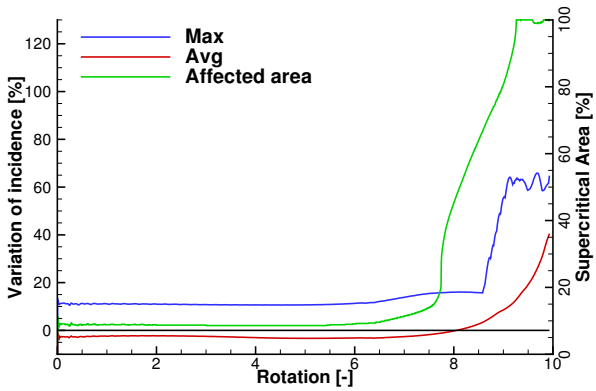

Figure 14: Variation of Incidence with a Steady Vortex Ingestion at Stall Inception with UBFM

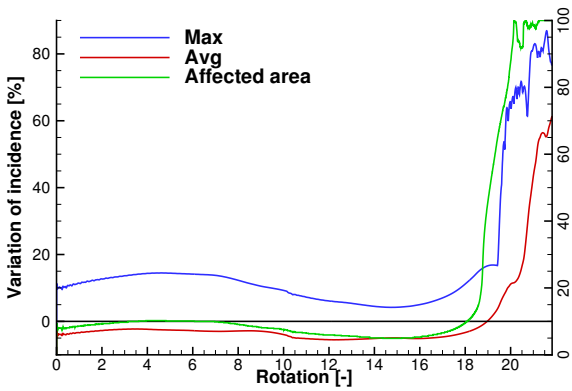

(a) 3Hz Circulation fluctuation

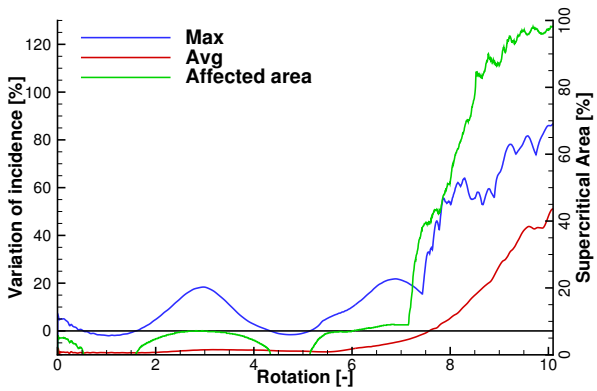

(b) 15Hz Vortex Core radius fluctuation

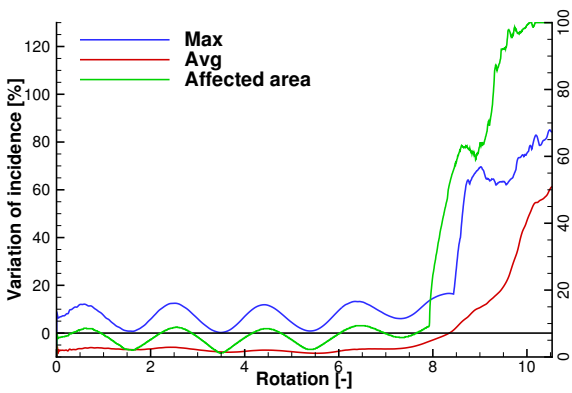

(c) 30Hz Circulation fluctuation

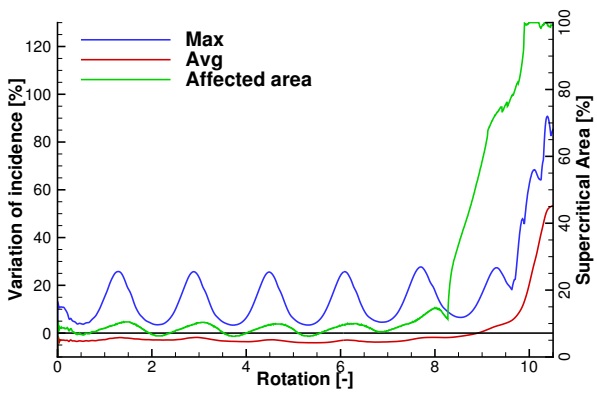

(d) 36Hz Vortex Core radius fluctuation

Figure 15: Effect of fluctuating vortex distortion on the overall incidence in the UBFM cases at Stall Inception

For the total signal fluctuation shown in Figure 16, the comparison between the URANS and UBFM simulation presents a similar behavior. Indeed, the criterion is valid in both the URANS and UBFM cases. In Figure 16b, a first increase in the affected area can be observed at 3.8 rotations due to the previous distortion peak at 2.8 rotations. The affected area then reverts back to the initial level at 5.5 rotation due to the reduction in the vortex intensity. This reaction of the affected area does not cause the average incidence to become positive. At 7.1 rotations, the increase in the affected area is more violent causing the average to become positive at 7.3 and rotating stall appears at 7.7 rotations. This is due to a sustained distortion level, and as for the cases in Figures 15b and 15c causes an entry in rotating stall in less that one rotation.

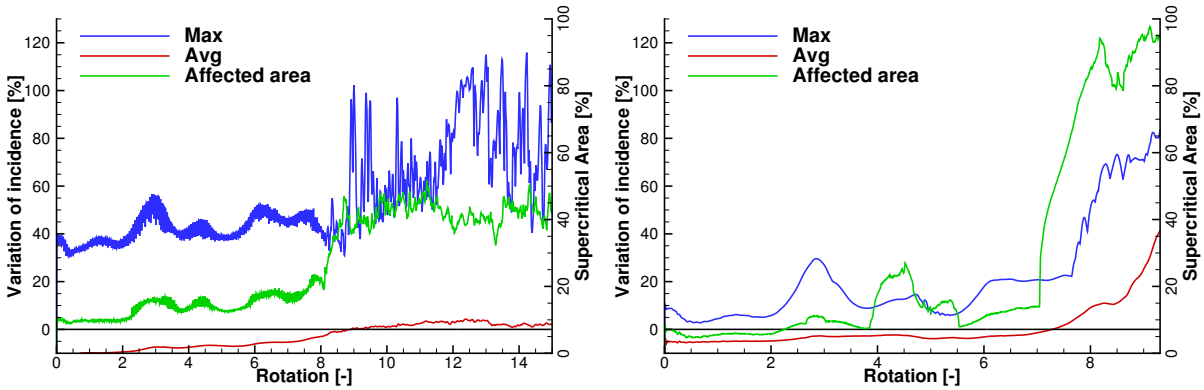

(a) Total Signal fluctuation URANS

(b) Total Signal fluctuation UBFM

Figure 16: Effect of the total signal fluctuatiation distortion on the overall incidence at Stall Inception

VIII. Discussion

The UBFM models exhibit an excellent near stall and rotating stall inception prediction for all the cases tested, *i.e.*, the clean inflow cases and with vortex distortion, with and without fluctuations. Indeed, the entry in rotating stall computations showed an excellent agreement with the reference data, with the correct rotational stall speed, number of lobes, and a sub 1% prediction of the throttle margin abatement in all but one case (1.19% for the total signal). The last stable point for the clean inflow as well as the steady vortex case is within 2% of throttle margin. For all simulations, the variation in incidence criterion is valid and the predicted critical angle using URANS is very similar to the UBFM cases. This means that this critical angle can be assessed using low-order simulations pending a correct calibration. A novel calibration method was presented and requires 3 to 4 single passage RANS points to obtain a very good agreement in the region of interest. The incidence criterion can predict the entry in rotating stall one rotation early even though the unsteadiness of the distortion could retard or advance this by up to, in the presented cases, 0.5 rotation. The criterion coupled with the UBFM methodology allows for the assessment of the operability of a fan as well as the entry in rotating stall characteristics in clean and distorted inflow conditions. Only minimal knowledge of the performance of the fan (3-4 single passage RANS computations), as well as the geometry, is required to use this UBFM methodology making it a powerful tool in the early design stages of a fan.

IX. Conclusion

The current computations are 26 times less costly than the URANS equivalent. Furthermore, the UBFM mesh and time-step could be further optimized and reductions of 30 times and possibly up to 40-50 times could be achieved. A novel calibration allowing for an excellent agreement near stall was presented and only relies on 3 to 4 single passage RANS simulations. The predictions of the last stable points and entry in rotating stall are in very good agreement in regards to the URANS reference. This means that the UBFM methodology can be efficiently used to quantify the impact of a distortion on the operability of a fan stage. Indeed, the model shows promising results both in terms of overall performance as well as rotating stall predictability where the stall inception point is within 1% of TM and the maximum total pressure ratio within 2% TM for the clean inflow case. The rotating stall cell number and speeds are similar to the URANS reference. For the other cases with the addition of a vortex, the maximum total pressure ratio is very well predicted and the reduction of the throttle margin at stall inception is within 0.6%. Moreover, the criterion based on the variation of incidence can be used in a design context, where a critical distortion could be determined based on the effect on the incidence of the fan. This method is conservative as the fan could operate momentarily beyond this critical incidence without stall but this might be frequency-dependent and not wise in real-world operations. Further work to relate the quadratic calibration to a physical phenomenon that can be introduced as a model could reduce the dependency on empirical data, this, as well as testing different and more complex distortion, will be necessary to prove this new methodology.

Acknowledgments

We would like to thank Safran Aircraft Engines for the funding, for supporting and for sharing valuable experimental data without which this research work would not have been possible. We also would like to thank Benjamin Godard, Alexandre Brosse and Jerôme Talbotec for their technical support and expertise along the working process.

References

[1]Awes, A., Brosse, A., Dufour, G., Carbonneau, X., and Godard, B., "EFFECT OF A VORTEX DISTORTION ON THE OPERABILITY OF AN ULTRA HIGH BYPASS RATIO FAN," *ASME Turbo Expo 2020*, No. GT2020-14596, June 2020.

[2]Kim, H. and Liou, M.-S., "Flow simulation and optimal shape design of N3-X hybrid wing body configuration using a body force method," *Aerospace Science and Technology*, Vol. 71, September 2017, pp. 661–674.

[3]Godard, J.-L., "SEMI-BURIED ENGINE INSTALLATION: THE NACRE PROJECT EXPERIENCE," *INTERNATIONAL CONGRESS OF THE AERONAUTICAL SCIENCES*, September 2010.

[4]Arntz, A. and Atinault, O., "Exergy-Based Performance Assessment of a Blended Wing–Body with Boundary-Layer Ingestion," *AIAA JOURNAL*, Vol. 53, No. 12, December 2015, pp. 3766.

[5]Arntz, A., Atinault, O., Destarac, D., and Merlen, A., "Exergy-based Aircraft Aeropropulsive Performance Assessment: CFD Application to Boundary Layer Ingestion," *32nd AIAA Applied Aerodynamics Conference*, No. AIAA 2014-2573, June 2014.

[6]Murphy, J., *Intake Ground Vortex Aerodynamics*, Ph.D. thesis, Cranfield University, 2008.

[7]Cao, T., Vadlamani, N. R., Tucker, P. G., Smith, A. R., Slaby, M., and Sheaf, C. T. J., "Fan Intake Interaction Under High Incidence," *Journal of Engineering for Gas Turbines and Power*, Vol. 139, April 2017, pp. 041204–1.

[8]Cui, J., Watson, R., Tucker, P., and Wilson, M., "LOW ORDER MODELLING FOR FAN AND OUTLET GUIDE VANES IN AERO-ENGINES," *ASME Turbo Expo 2018*, No. GT2018-75660, June 2018.

[9]Marble, F. E., "Three-Dimensional Flow in Turbomachines," *High Speed Aerodynamics and Jet Propulsion*, Vol. 10, 1964, pp. 83–166.

[10]Gong, Y., *A computational model for rotating stall and inlet distortions in multistage compressors*, Ph.D. thesis, Massachusetts Institute of Technology. Dept. of Aeronautics and Astronautics, Febuary 1999.

[11]Thollet, W., *Body force modeling of fan-airframe interactions*, Ph.D. thesis, Institut Supérieur de l'Aéronautique et de l'Espace (ISAE-SUPAERO), Juillet 2017.

[12]Hall, D. K., *Analysis of Civil Aircraft Propulsors with Boundary Layer Ingestion*, Ph.D. thesis, MASSACHUSETTS INSTITUTE OF TECHNOLOGY, Febuary 2015.

[13]J. Day, I., "Stall Inception in Axial Flow Compressors," *Journal of Turbomachinery*, Vol. 115, 01 1993.

[14]Camp, T. R. and Day, I. J., "A Study of Spike and Modal Stall Phenomena in a Low- Speed Axial Compressor," *Journal of Turbomachinery*, Vol. 120, July 1998, pp. 393.

[15]Vo, H. D., Tan, C. S., and Greitzer, E. M., "Criteria for Spike Initiated Rotating Stall," *Journal of Turbomachinery*, Vol. 130, January 2008, pp. 011023–1.

[16]Pullan, G., Young, A. M., Day, I. J., Greitzer, E. M., and Spakovszky, Z. S., "Origins and Structure of Spike-Type Rotating Stall," *Journal of Turbomachinery*, Vol. 137, May 2015, pp. 051007–1.

[17]Perovic, D., Hall, C. A., and Gunn, E. J., "Stall Inception in a Boundary Layer Ingesting Fan," *Journal of Turbomachinery*, Vol. 141, No. 9, June 2019.

[18]Chima, R. V., "A THREE-DIMENSIONAL UNSTEADY CFD MODEL OF COMPRESSOR STABILITY," *ASME Turbo Expo*, No. GT2006-90040, May 2006, pp. pp. 1157–1168.

[19]Gong, Y., Tan, C. S., Gordon, K. A., and Greitzer, E. M., "A Computational Model for Short-Wavelength Stall Inception and Development in Multistage Compressors," *Journal of Turbomachinery*, Vol. 121, October 1999, pp. 726.

[20]Thollet, W., Dufour, G., and Carbonneau, X., "Assessment of body force methodologies for the analysis of intake-fan aerodynamic interactions," *Proceedings of ASME Turbo Expo 2016*, No. GT2016-57014, 2016.

[21]Cambier, L., Heib, S., and Plot, S., "The Onera elsA CFD software: input from research and feedback from industry," *Mechanics & Industry*, Vol. 14, No. 3, 2013, pp. 159–174.

[22]Benoit, C., Péron, S., and Landier, S., "Cassiopee: a CFD pre-and post-processing tool," *Aerospace Science and Technology*, Vol. 45, 2015, pp. 272–283.